

Washington University School of Medicine

Digital Commons@Becker

---

Open Access Publications

---

9-1-2020

## Imaging features of neonatal systemic juvenile xanthogranuloma: A case report and review of the literature

Siping He

Ke Jin

Xicheng Deng

Zhengzhen Zhou

Robert C McKinstry

*See next page for additional authors*

Follow this and additional works at: [https://digitalcommons.wustl.edu/open\\_access\\_pubs](https://digitalcommons.wustl.edu/open_access_pubs)

---

---

**Authors**

Siping He, Ke Jin, Xicheng Deng, Zhengzhen Zhou, Robert C McKinstry, and Yong Wang

---

# Imaging features of neonatal systemic juvenile xanthogranuloma: a case report and review of the literature

Journal of International Medical Research  
48(9) 1–9

© The Author(s) 2020

Article reuse guidelines:

[sagepub.com/journals-permissions](https://sagepub.com/journals-permissions)

DOI: 10.1177/0300060520956416

[journals.sagepub.com/home/imr](https://journals.sagepub.com/home/imr)

Siping He<sup>1</sup> , Ke Jin<sup>1</sup>, Xicheng Deng<sup>2</sup> ,  
Zhengzhen Zhou<sup>3</sup>, Robert C McKinstry<sup>4</sup> and  
Yong Wang<sup>5</sup>

## Abstract

Juvenile xanthogranuloma (JXG) is the most common non-Langerhans cell histiocytic disorder in children. This report describes the case of a 28-day-old boy that presented with multiple subcutaneous nodular lesions on the trunk and extremities, and multiple red nodular lesions on the scrotum. Magnetic resonance imaging (MRI) of the brain showed a well-demarcated extra-axial dura-based mass that appeared isointense or slightly hyperintense on T1-weighted images, hypointense on T2-weighted images and had intense enhancement on gadolinium-enhanced T1-weighted images. Computed tomography (CT) or MRI scans of the chest and abdomen revealed multiple scattered nodular or patchy lesions of varying sizes in the lungs, liver and left kidney. Histological analysis of a subcutaneous mass suggested JXG. The patient was diagnosed with neonatal systemic JXG with involvement of the central nervous system, lungs, liver, kidneys, subcutaneous soft tissue and skin. CT and MRI after 3 months of treatment with methylprednisolone sodium succinate demonstrated that the lesions were obviously diminished. This report discusses the imaging findings in this current case of multi-organ JXG and reviews the imaging literature on this condition to improve awareness of the lesions in order to help radiologists establish an accurate differential diagnosis when confronted with similar cases.

<sup>1</sup>Department of Radiology, Hunan Children's Hospital, Changsha, Hunan Province, China

<sup>2</sup>Department of Cardiothoracic Surgery, Hunan Children's Hospital, Changsha, Hunan Province, China

<sup>3</sup>Department of Pathology, Hunan Children's Hospital, Changsha, Hunan Province, China

<sup>4</sup>Mallinckrodt Institute of Radiology, Washington University, St. Louis, MO, USA

<sup>5</sup>Department of Obstetrics & Gynecology, Washington University, St. Louis, MO, USA

### Corresponding author:

Yong Wang, Department of Obstetrics & Gynecology, School of Medicine, Washington University in St. Louis, 4901 Forest Park Avenue Suite 10201, COH, St. Louis, MO 63108, USA.

Email: [wangyong@wustl.edu](mailto:wangyong@wustl.edu)



## Keywords

juvenile xanthogranuloma, non-Langerhans histiocytosis, neonatal, computed tomography, magnetic resonance imaging

Date received: 6 April 2020; accepted: 13 August 2020

## Introduction

Juvenile xanthogranuloma (JXG, also called nevoxanthoendothelioma) is the most common non-Langerhans cell histiocytic disorder in children.<sup>1</sup> JXG, which is caused by the proliferation or activation of interstitial/dermal dendritic cells and macrophages, occurs predominantly in infancy and early childhood.<sup>2</sup> JXG mainly affects the skin and patients typically present with multiple cutaneous papules or nodules.<sup>3</sup> However, between 3.9% and 5.0% of patients have lesions in extracutaneous organs, including the liver, spleen, lungs, kidneys, eyes, subcutaneous soft tissue, bones and central nervous system (CNS).<sup>2,4,5</sup> Clinically, JXG is divided into cutaneous JXG, which only affects the skin, and systemic JXG, which can affect multiple extracutaneous organs with or without skin lesions.<sup>4</sup> Cutaneous JXG follows a benign course without treatment.<sup>6</sup> In contrast, systemic JXG can be associated with complications that necessitate aggressive medical care and imaging to monitor extracutaneous lesions.<sup>5</sup> A revised classification system recently proposed to include Langerhans cell histiocytosis (LCH), Erdheim-Chester disease (ECD) and extracutaneous JXG in the Langerhans group and to consider as ECD all extracutaneous or disseminated JXG with a gain-of-function mutation of the *BRAF*, *NRAS*, *KRAS* or *MAP2K1* (grade D2) genes.<sup>7</sup> It has also been reported that more than half of patients with ECD and LCH have *BRAF*<sup>V600E</sup> mutations; and mutations

affecting the mitogen-activated protein kinase pathway and phosphatidylinositol 3-kinase/protein kinase B pathway are present in a large proportion of patients with wild-type *BRAF* mutation.<sup>8</sup> Mitogen-activated protein kinase kinase enzyme (MEK) inhibitors and combined anti-*BRAF* and anti-*MEK* therapies also appear promising.<sup>8</sup>

This current report describes a case of neonatal systemic JXG with involvement of the CNS, lungs, liver, kidneys, subcutaneous soft tissue and skin. This report also reviews the imaging literature on this condition and discusses the imaging findings of JXG with multiple organ involvement to improve awareness of the lesions. This report may help radiologists establish an accurate differential diagnosis when confronted with similar cases.

## Case report

A 28-day-old boy presented to the Department of Radiology, Hunan Children's Hospital, Changsha, Hunan Province, China in August 2018 with multiple subcutaneous nodular lesions on the trunk and extremities, and multiple red nodular lesions on the scrotum. The subcutaneous lesions were firm, the boundaries were clear, and there were no adhesions to the surrounding tissue. The largest lesion, located on the right chest wall, measured approximately  $2.5 \times 2.0 \times 1.5$  cm (Figure 1). On examination, the boy had no focal neurological deficits or evidence



**Figure 1.** A subcutaneous nodular lesion located on the right chest wall (arrow) of a 28-day-old boy that presented with multiple subcutaneous nodular lesions on the trunk and extremities, and multiple red nodular lesions on the scrotum.

of hepatosplenomegaly or superficial lymph adenopathy. Laboratory results on admission showed: haemoglobin 93.0 g/l; total protein 39.1 g/l; albumin 25.8 g/l; globulin 13.3 g/l; alpha-1-fetoprotein 2679.8 ng/ml. To define the extent of the disease, brain and abdominal magnetic resonance imaging (MRI) and chest and abdominal computed tomography (CT) were performed.

The MRI of the brain showed a well-demarcated extra-axial dura-based lesion with mass effect on the right temporal lobe, measuring approximately  $1.8 \times 1.3 \times 1.7$  cm. The mass appeared isointense or slightly hyperintense on T1-weighted images (Figure 2A). The lateral portion of the mass was slightly hypointense, and the medial portion of the mass was hypointense on T2-weighted images (Figure 2B) and showed slightly restricted diffusion on diffusion-weighted images (DWI) (Figures 2C and 2D). The mass was intense and homogeneously enhanced and demonstrated a dural tail sign after intravenous gadolinium administration (Figure 2E).

A CT scan of the chest revealed multiple bilateral peripheral pulmonary nodules of varying sizes. The largest nodule, located

on the posterior aspect of the lower lobe of the left lung, measured approximately  $0.8 \times 0.9 \times 0.7$  cm (Figures 3A and 3B). A sharply circumscribed subcutaneous mass in the right chest wall was present, appearing as a homogeneous, solid soft-tissue mass without calcification and isoattenuating compared with muscle, measuring approximately  $1.1 \times 2.1 \times 1.7$  cm. A contrast-enhanced CT scan of the abdomen revealed multiple scattered nodular or patchy hypodense lesions of varying sizes in the liver and left kidney and partial lesions distributed along the portal vein (Figures 3C–3H).

In MRI of the liver, T1-weighted images showed lesions with signal intensity similar to or less than that of the surrounding liver parenchyma (Figure 4A) and T2-weighted images showed lesions with slightly high intensity (Figure 4B). In DWI, the nodule located on the right liver subcapsular region showed slightly restricted diffusion, and curvilinear high intensity was present along the periportal vein, and in an apparent diffusion coefficient map, they appeared hypointense (Figures 4C and 4D). The largest kidney lesion had ill-defined margins and measured approximately  $1.2 \times 1.3 \times 0.9$  cm. In MRI of the kidney, T1-weighted images showed lesions with signal intensity slightly higher than that of the surrounding renal parenchyma and T2-weighted images showed lesions with slightly low intensity (Figure 4E). In DWI, the lesions appeared hyperintense, and in an apparent diffusion coefficient map, they appeared hypointense (Figures 4F and 4G).

Histological analysis of biopsies of the subcutaneous lesions located on the right lower leg and forearm revealed a large amount of monocytoid histiocytes, inflammatory cell infiltrates and Touton giant cells (Figure 5A). Immunohistochemical staining revealed that the lesion was strongly positive for CD163 (Figure 5B) and vimentin and negative for Ki-67, CD1a,

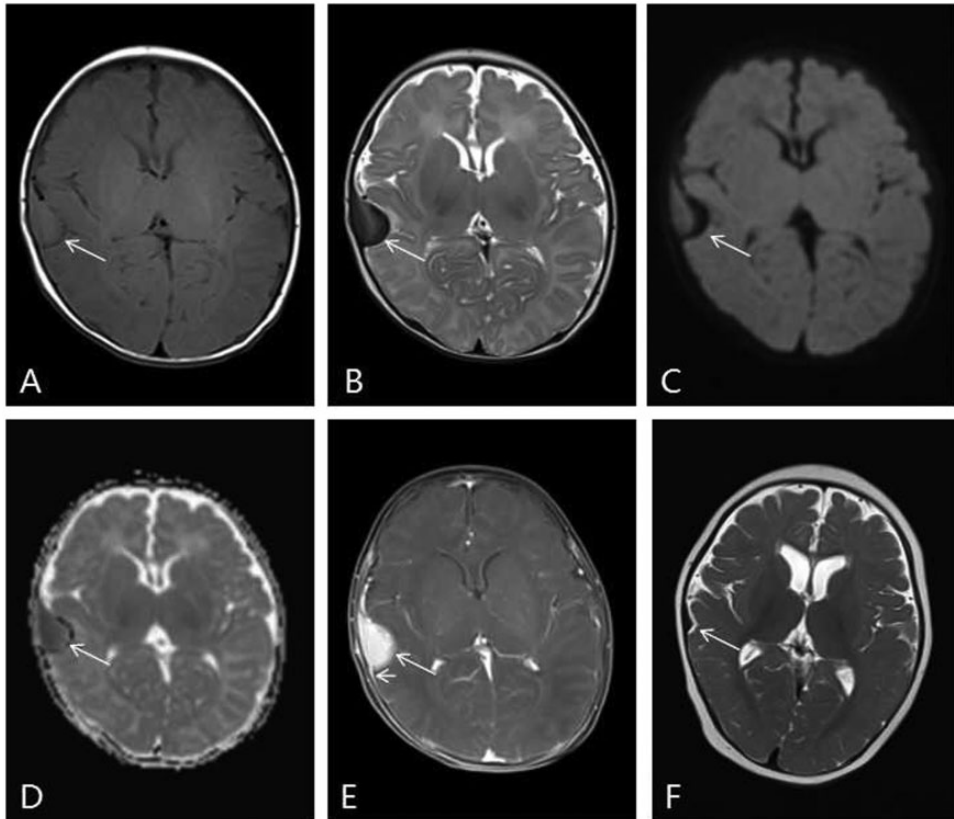


**Figure 2.** Brain magnetic resonance imaging scans of a 28-day-old boy that presented with multiple subcutaneous nodular lesions on the trunk and extremities, and multiple red nodular lesions on the scrotum. (A) An axial T1-weighted image shows an extra-axial dura-based isointense lesion (arrow) with mass effect on the right temporal lobe. (B) An axial T2-weighted image shows that the lateral portion of the mass was hypointense and the medial portion of the mass was hypointense (arrow). (C and D) Diffusion-weighted images show that the lateral portion of the mass had slightly restricted diffusion (arrows). (E) A T1-weighted post-contrast axial image shows that the mass had intense homogenous enhancement (arrow) and demonstrated a dural tail sign (short arrow). (F) After 3 months of treatment, the lesion was significantly smaller.

S100 and Langerin. Together, the histology and immunohistochemical profile of this lesion was consistent with JXG. Whole exome sequencing and phospho-extracellular signal-related kinase staining were not performed.

The patient was treated with 12 mg methylprednisolone sodium succinate by intravenous drip once a day for 3 days and 12 mg methylprednisolone tablets orally once a day for 12 weeks. After

3 months, MRI and CT re-examinations revealed that the lesions were significantly smaller than at the initial examination (Figure 2F, 3I, 4H and 4I). This study was approved by the Institutional Review Board Committee at Hunan Children's Hospital (no. HCHLL-2020-13). The parents of the patient participating in the study provided written informed consent for this case report to be published.

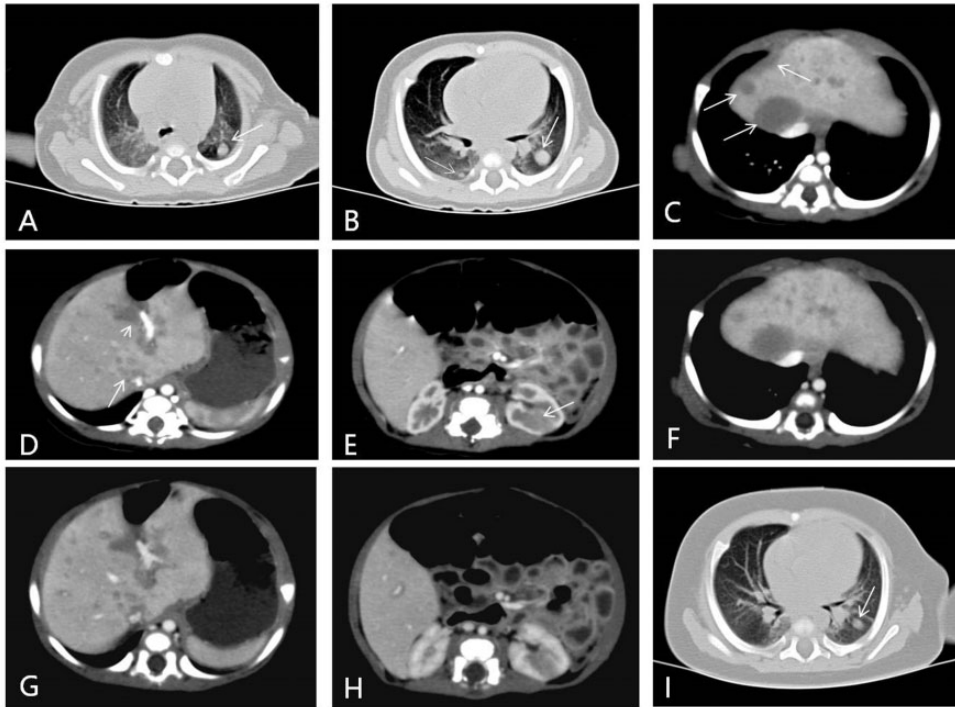


**Figure 3.** Lung, liver and kidney computed tomography (CT) images of a 28-day-old boy that presented with multiple subcutaneous nodular lesions on the trunk and extremities, and multiple red nodular lesions on the scrotum. (A and B) Axial CT images of the chest (lung window) demonstrate multiple bilateral peripheral pulmonary nodules of varying sizes (arrows). (C, D and E) Axial contrast-enhanced abdominal CT images (arterial phase) demonstrate multiple scattered nodules or patchy hypodense lesions (arrows) in the liver and left kidney that were mildly enhanced. Partial hepatic lesions were distributed along the portal vein (short arrow). (F, G and H) Axial contrast-enhanced abdominal CT images (venous phase) demonstrate multiple scattered nodules or patchy hypodense lesions in the liver and left kidney. (I) After 3 months of treatment, the lesions in the lung were significantly smaller.

## Discussion

The imaging findings from this current case were similar to reports in the literature in many ways but differed in a few aspects that might be helpful to radiologists when differentially diagnosing JXG. This discussion will focus on a few of those key similarities and differences.

In published reports,<sup>9,10</sup> the appearance of intracranial JXG lesions on MRI varies. Lesions are usually round and are hypointense, isointense or slightly hyperintense on T1-weighted or T2-weighted images. Lesions appear with or without

surrounding oedema, show restricted diffusion on DWI, and can have either homogeneous or heterogeneous enhancement on gadolinium-enhanced T1-weighted images. A previous report suggested that JXG diagnosis could be suggested by the presence of a soft-tissue mass with high signal intensity on T1-weighted images, lower signal intensity on T2-weighted images than in the cerebral cortex, homogeneous enhancement and decreased diffusivity.<sup>9</sup> The current case was consistent with this description. The isointensity or slight hyperintensity in T1-weighted images in lesions compared

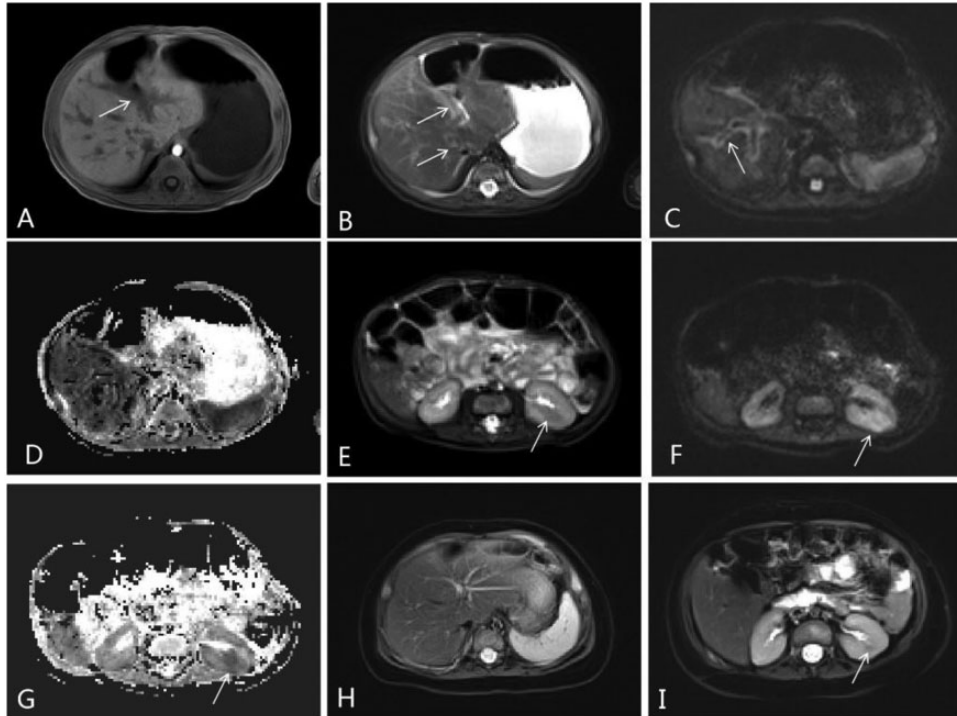


**Figure 4.** Liver and kidney magnetic resonance imaging scans of a 28-day-old boy that presented with multiple subcutaneous nodular lesions on the trunk and extremities, and multiple red nodular lesions on the scrotum. (A) An axial T1-weighted image shows lesions with signal intensity similar to or less than that of the surrounding liver parenchyma (arrows). (B) An axial T2-weighted image shows lesions with slightly high intensity (arrows). (C and D) Diffusion-weighted images show curvilinear high intensity along the periportal vein (arrow) and hypointensity in an apparent diffusion coefficient map. (E) An axial T2-weighted image shows lesions with slightly low intensity than that of the surrounding renal parenchyma (arrow). (F and G) Diffusion-weighted images reveal high signal and an apparent diffusion contrast map reveals a low signal, confirming diffusion restriction in the lesions (arrow). (H and I) After 3 months of treatment, the lesions in the liver and kidney were significantly smaller.

with the cortex is presumably attributable to the presence of lipid within the lesions. Additionally, the hypointensity on T2-weighted images and decreased diffusivity may be attributable to reduced cellularity or collagenous matrix.<sup>9</sup> This issue cannot be addressed in the current case because the intracranial lesion was not analysed histologically.

Several papers have reported JXG lesions in the lungs.<sup>2,3,11-13</sup> Patients with pulmonary lesions commonly have systemic

disease and a worse prognosis than patients without pulmonary lesions.<sup>11</sup> On chest CT, JXG lesions in the lung usually appear as bilateral, diffuse micro- or macronodules.<sup>3,12,13</sup> Consistent with this description, chest CT in the current case revealed multiple bilateral peripheral pulmonary nodules of varying sizes. However, a previous report noted that JXG lesions in the lung can have an interstitial pattern with accompanying micronodules and mediastinal and hilar lymphadenopathy and suggested that



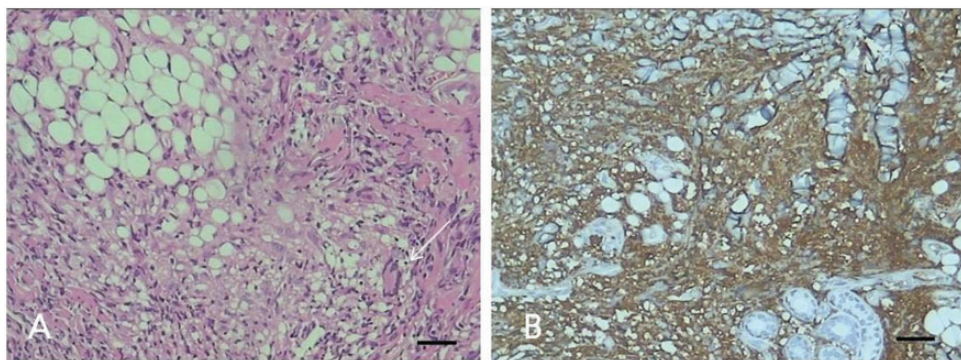


**Figure 5.** Histological analysis of biopsies of the subcutaneous lesions located on the right lower leg and forearm of a 28-day-old boy revealed a large amount of monocytoïd histiocytes, inflammatory cell infiltrates and Touton giant cells. (A) Haematoxylin and eosin staining shows multi-regional histology and Touton giant cells (arrow). (B) Immunohistochemical staining demonstrated that the lesion was strongly positive for CD163 (shown in the image) and vimentin and negative for S100 and Langerin. Scale bar 50  $\mu$ m. The colour version of this figure is available at: <http://imr.sagepub.com>.

such imaging findings should prompt radiologists to consider JXG in the differential diagnosis.<sup>3</sup>

Previous reports have described JXG lesions in the kidney as isodense masses that appeared hypodense in contrast-enhanced CT.<sup>3,13</sup> Consistent with this, scattered nodular or patchy hypodense lesions of varying sizes were observed in the left kidney in the current case on contrast-enhanced CT. In MRI, T2-weighted images showed lesions with slightly low intensity and T1-weighted images showed lesions with signal intensity slightly higher than that of the surrounding renal parenchyma. Lesions were hyperintense on DWI and hypointense in an apparent diffusion coefficient map, which may be related to the accumulation of cells derived from the monocyte and macrophage lineages, infiltration of inflammatory cells, increased cell density and viscosity, resulting in the restricted diffusion of water molecules. To the best of our knowledge, this is the first report of such features of renal JXG lesions. Although such findings are likely not characteristic, they may provide some clues for diagnosis.

In the liver, JXG lesions have been described as masses of soft-tissue attenuation with minimal enhancement on CT.<sup>14</sup> Additionally, MRI shows slightly high signal intensity on T2-weighted images and either slightly high or low signal intensity on T1-weighted images.<sup>3,13,15</sup> A previous report noted that on the venous phase, a liver lesion was hypovascular and had a central area of low attenuation, and the hepatic lesions did not lose signal intensity on opposed-phase compared with in-phase gradient-echo images.<sup>15</sup> Partial lesions distributed along the portal vein that were slightly hyperintense on T2-weighted images and slightly hypointense on T1-weighted images were observed in the current case. This current finding may be similar to a JXG autopsy finding in which histiocytes in the portal tract spilled over into the adjacent lobule.<sup>16</sup> In DWI in the current case, the nodule located on the right liver subcapsular region showed slightly restricted diffusion and curvilinear high intensity was present along the periportal vein. To the best of our knowledge, the MRI

appearance of lesions in the liver has not been described previously.

The diagnosis of JXG relies on clinical and histopathological examinations. From an imaging standpoint, the major differential diagnoses for this current case were LCH, infectious disease, multiple organ metastases from a malignant tumour and tuberous sclerosis complex. Intracranial involvement in LCH and JXG may have a similar appearance, but liver involvement in LCH usually shows hepatic parenchymal cyst-like lesions, alternative stenoses and dilatation of the intrahepatic ducts.<sup>17</sup> Additionally, in LCH, early imaging findings of lung involvement include multiple nonspecific pulmonary nodules, which cavitate into cysts over time.<sup>18</sup> Infectious lesions may be ruled out by the imaging findings of intracranial lesions and laboratory results. To diagnose multi-organ metastasis from a malignant tumour, the primary tumour can be found. In neonatal neuroblastoma, the primary tumour site is most commonly in the adrenal gland. In neonatal tuberous sclerosis complex, intracranial involvement often manifests as subventricular and subcortical multiple nodules, and the most common liver and renal anomalies are the presence of angiomyolipomas.

In conclusion, JXG can involve multiple extracutaneous organs and has a variety of imaging manifestations. This current report presents the imaging features of JXG with involvement of the CNS, lungs, liver, kidney and subcutaneous soft tissue. Familiarity with the common locations and imaging appearances may prompt radiologists to establish a more accurate differential diagnosis for JXG. However, a limitation of this case report was that there was no genomic profiling to generate options for targeted therapies.


#### Declaration of conflicting interest

The authors declare that there are no conflicts of interest

#### Funding

This study was supported by a grant from the Natural Science Foundation of Hunan Province (no. 2019JJ40156). Robert C. McKinstry and Yong Wang were supported by a research grant from March of Dimes (no. 22-FY19-344).

#### ORCID iDs

Siping He  <https://orcid.org/0000-0002-4819-8437>

Xicheng Deng  <https://orcid.org/0000-0002-2935-5724>

#### Reference

1. Ladisch S and Jaffe ES. The histiocytoses. In: Pizzo PA and Poplack DC (eds) *Principles and practice of pediatric oncology*. Philadelphia: Lippincott, 1993, pp.617–631.
2. Janssen D and Harms D. Juvenile xanthogranuloma in childhood and adolescence: a clinicopathologic study of 129 patients from the Kiel Pediatric Tumor Registry. *Am J Surg Pathol* 2005; 29: 21–28.
3. Bakir B, Unuvar E, Terzibasoglu E, et al. Atypical lung involvement in a patient with systemic juvenile xanthogranuloma. *Pediatr Radiol* 2007; 37: 325–327.
4. Dehner LP. Juvenile xanthogranulomas in the first two decades of life: a clinicopathologic study of 174 cases with cutaneous and extracutaneous manifestations. *Am J Surg Pathol* 2003; 27: 579–593.
5. Freyer DR, Kennedy R, Bostrom BC, et al. Juvenile xanthogranuloma: forms of systemic disease and their clinical implications. *J Pediatr* 1996; 129: 227–237.
6. Gianotti F and Caputo R. Histiocytic syndromes: a review. *J Am Acad Dermatol* 1985; 13: 383–404.
7. Emile JF, Ablu O, Fraitag S, et al. Revised classification of histiocytoses and neoplasms of the macrophage-dendritic cell lineages. *Blood* 2016; 127: 2672–2681.
8. Haroche J, Cohen-Aubart F and Rollins BJ. Histiocytoses: emerging neoplasia behind inflammation. *Lancet Oncol* 2017; 18: e113–e125.
9. Ginat DT, Vargas SO, Silvera VM, et al. Imaging Features of Juvenile

- Xanthogranuloma of the Pediatric Head and Neck. *AJNR Am J Neuroradiol* 2016; 37: 910–916.
10. Pagura L, de Prada I, López-Pino MA, et al. Isolated intracranial juvenile xanthogranuloma. A report of two cases and review of the literature. *Childs Nerv Syst* 2015; 31: 493–498.
  11. Pfeifer K, Mian A, Adebawale A, et al. Radiographic and Pathologic Manifestations of Uncommon and Rare Pulmonary Lesions. *Can Assoc Radiol J* 2016; 67: 179–189.
  12. Lottsfeldt FI and Good RA. Juvenile xanthogranuloma with pulmonary lesions. A case report. *Pediatrics* 1964; 33: 233–238.
  13. Patel P, Vyas R, Blickman J, et al. Multimodality imaging findings of disseminated juvenile xanthogranuloma with renal involvement in an infant. *Pediatr Radiol* 2010; 40(Suppl 1): S6–S10.
  14. Guthrie JA and Arthur RJ. Case report: juvenile xanthogranuloma with pulmonary, subcutaneous and hepatic involvement. *Clin Radiol* 1994; 49: 498–500.
  15. Yeh BM, Nobrega KTM, Reddy GP, et al. Juvenile xanthogranuloma of the heart and liver: MRI, sonographic, and CT appearance. *AJR Am J Roentgenol* 2007; 189: W202–W204.
  16. Rodriguez-Velasco A, Rodriguez-Zepeda MDC and Ortiz-Hidalgo C. Infantile systemic juvenile xanthogranuloma case with massive liver infiltration. *Autops Case Rep* 2019; 9: e2018081.
  17. Kaplan KJ, Goodman ZD and Ishak KG. Liver involvement in Langerhans' cell histiocytosis: a study of nine cases. *Mod Pathol* 1999; 12: 370–378.
  18. Abbott GF, Rosado-de-Christenson ML, Franks TJ, et al. From the archives of the AFIP: Pulmonary Langerhans cell histiocytosis. *Radiographics* 2004; 24: 821–841.